Geotechnical Characteristics and Slope Stability Analysis on the Deeper Slope of the Ligurian Margin, Southern France

Fei Ai, Annika Förster, Sylvia Stegmann, and Achim Kopf

Abstract

Submarine slope failures of various types and sizes are common along the tectonic and seismically active Ligurian margin, northwestern Mediterranean Sea, primarily because of seismicity up to ~M6, rapid sediment deposition in the Var fluvial system, and steepness of the continental slope (average 11°). We present geophysical, sedimentological and geotechnical results of two distinct slides in water depth >1,500 m: one located on the flank of the Upper Var Valley called Western Slide (WS), another located at the base of continental slope called Eastern Slide (ES). WS is a superficial slide characterized by a slope angle of ~4.6° and shallow scar (~30 m) whereas ES is a deep-seated slide with a lower slope angle (~3°) and deep scar (~100 m). Both areas mainly comprise clayey silt with intermediate plasticity, low water content (30–75 %) and underconsolidation to strong overconsolidation. Upslope undeformed sediments have low undrained shear strength (0–20 kPa) increasing gradually with depth, whereas an abrupt increase in strength up to 200 kPa occurs at a depth of ~3.6 m in the headwall of WS and ~1.0 m in the headwall of ES. These boundaries are interpreted as earlier failure planes that have been covered by hemipelagite or talus from upslope after landslide emplacement.

Infinite slope stability analyses indicate both sites are stable under static conditions; however, slope failure may occur in undrained earthquake condition. Peak earthquake acceleration from 0.09 g on WS and 0.12 g on ES, i.e. M5–5.3 earthquakes on the spot, would be required to induce slope instability. Different failure styles include rapid sedimentation on steep canyon flanks with undercutting causing superficial slides in the west and an earthquake on the adjacent Marcel fault to trigger a deep-seated slide in the east.

F. Ai (✉)
MARUM-Center for Marine Environmental Sciences, University of Bremen, Leobener Straße, 28359 Bremen, Germany

Faculty of Geosciences, University of Bremen, Leobener Straße, 28359 Bremen, Germany

State Key Laboratory of Geomechanics and Geotechnical Engineering, Institute of Rock and Soil Mechanics, Chinese Academy of Sciences, 430071 Wuhan, China
e-mail: aifei@uni-bremen.de

A. Förster
Institute of Geosciences and Geography, Martin-Luther-University Halle-Wittenberg, von Seckendorff Platz 3, 06120 Halle (Saale), Germany
e-mail: annika.foerster@geo.uni-halle.de

S. Stegmann • A. Kopf
MARUM-Center for Marine Environmental Sciences, University of Bremen, Leobener Straße, 28359 Bremen, Germany

Faculty of Geosciences, University of Bremen, Leobener Straße, 28359 Bremen, Germany
e-mail: stegmann@uni-bremen.de; akopf@uni-bremen.de

Introduction

Submarine slope failures represent the main agents of sediment transport from continental slope to deep ocean, and one of the most common geohazards impacting on both offshore infrastructures (e.g. pipeline, cables and platforms) and costal areas (e.g. slope failure-induced tsunamis) (Locat and Lee 2002). Slope failures are generally controlled by long-term preconditioning factors (e.g. high sedimentataion rate, weak layer and oversteepening) and short-term triggering mechanisms (e.g. earthquake, anthropogenic activity) (Sultan et al. 2004). However, the exact causes for the different slope failure styles are still poorly understood.

The Ligurian margin, northwestern Mediterreanean Sea, is one of most intensely studied natural laboratories for landslide initiation in seismically active areas because of its steep topography with numerous landslide scars of different size. Previous slope stability analyses in the region mainly focused on the 1979 Nice Airport Slide or the upper slope of Ligurian margin (Cochonat et al. 1993; Mulder et al. 1994; Sultan et al. 2004; Dan et al. 2007; Leynaud and Sultan 2010; Stegmann et al. 2011). This study presents two distinct slides (WS and ES) along the deeper slope of Ligurian margin (1,500–2,000 m below seaflow (mbsf)). Klaucke and Cochonat (1999) and Migeon et al. (2011) concentrated on the mophologies of slope failure and qualitatively identified their triggering mechanisms. Kopf et al. (2008) and Förster et al. (2010) charatererized the architecture and evolution of the slope failures. Our study presents geotechnical properties of sediments from undeformed, headwall and deposit areas of WS and ES. Those results are used for infinite slope stability of undeformed sediments under various conditions to (1) identify the preconditioning factors and (2) quantify the influence of earthquakes as a key factor in slope failing mechanisms in this densely populated area.

Geological, Geomorphological and Lithological Setting

The Ligurian Basin is considered as a back-arc basin, that formed by continental rifting and drifting during the late Oligocene from the southeastward rollback of the Apennines-Maghrebides subduction zone (Larroque et al. 2012 and references therein). Currently, active basin deformation occurs offshore at a slow rate of ~1.1 m/ka NNW-SSE, which involves moderate seismic activity with common earthquake magnitudes of M2.2 to M4.5 (Fig. 1a). However, earthquake magnitudes up to M6.8 (e.g. 1887 Ligurian earthquake) are documented at the Ligurian margin (Larroque et al. 2012). The Marcel Fault shows evidence of present activity that three moderate earthquakes (M3.8–M4.6) took place around this fault over the last 30 years (Larroque et al. 2012 and Fig. 1b).

The northern upper continental slope of the Ligurian Basin is eroded by two major canyons (Var canyon and Paillon canyon), which coalesce at a depth of 1,650 m (Cochonat et al. 1993 and Fig. 1b). A single channel was formed at the confluence of the two canyons and divided into three parts: upper, middle and lower valleys. The walls of Upper Valley are highly dissected by small retrogressive failure events (Migeon et al. 2011) such as that west of Cap Ferrat Ridge called Western Slide (WS). It is characterized by shallow headwalls (<30 m) with high slope gradients of ~4.6° (Fig. 1c and Fig. 2a). A slope failure east of Cap Ferrat Ridge is termed Eastern slide (ES) and shows deep slide scars (80–120 m) and a lower slope gradient of ~3° (Fig. 1c and Fig. 2b).

Recent processes of sediment transport and deposition in the Var Upper Valley were mainly dominated by hyperpycnal-flow activity, failure-induced turbidity currents, and hemipelagite emplacement (Migeon et al. 2011). The lithostratigraphic succession of WS is characterized by homogenous, fine-grained hemipelagic clayey silt with some coarse-grained sand intervals (Kopf et al. 2008 and Fig. 3a). Areas east of Cap Ferrat Ridge are not connected to major fluvial input of the Var system and receive only hemipelagic sediments (Klaucke et al. 2000). The sediments are generally composed of well-bioturbated, homogenous, fine-grained hemipelagic deposits (Kopf and Cruise 2008 and Fig. 3b).

Materials and Methods

Laboratory Tests

The principal data set for this study is based on six gravity cores from undeformed slope, headwall and deposit areas of the WS and ES events. Water content was measured by a GeoTeK Multi Sensor Core Logger (MSCL) on the archive halves at 2 cm intervals. Undrained shear strength (S_u) was estimated using a Mennerich Geotechnik (Germany) vane shear apparatus and Wykeham Farrance cone penetrometer.
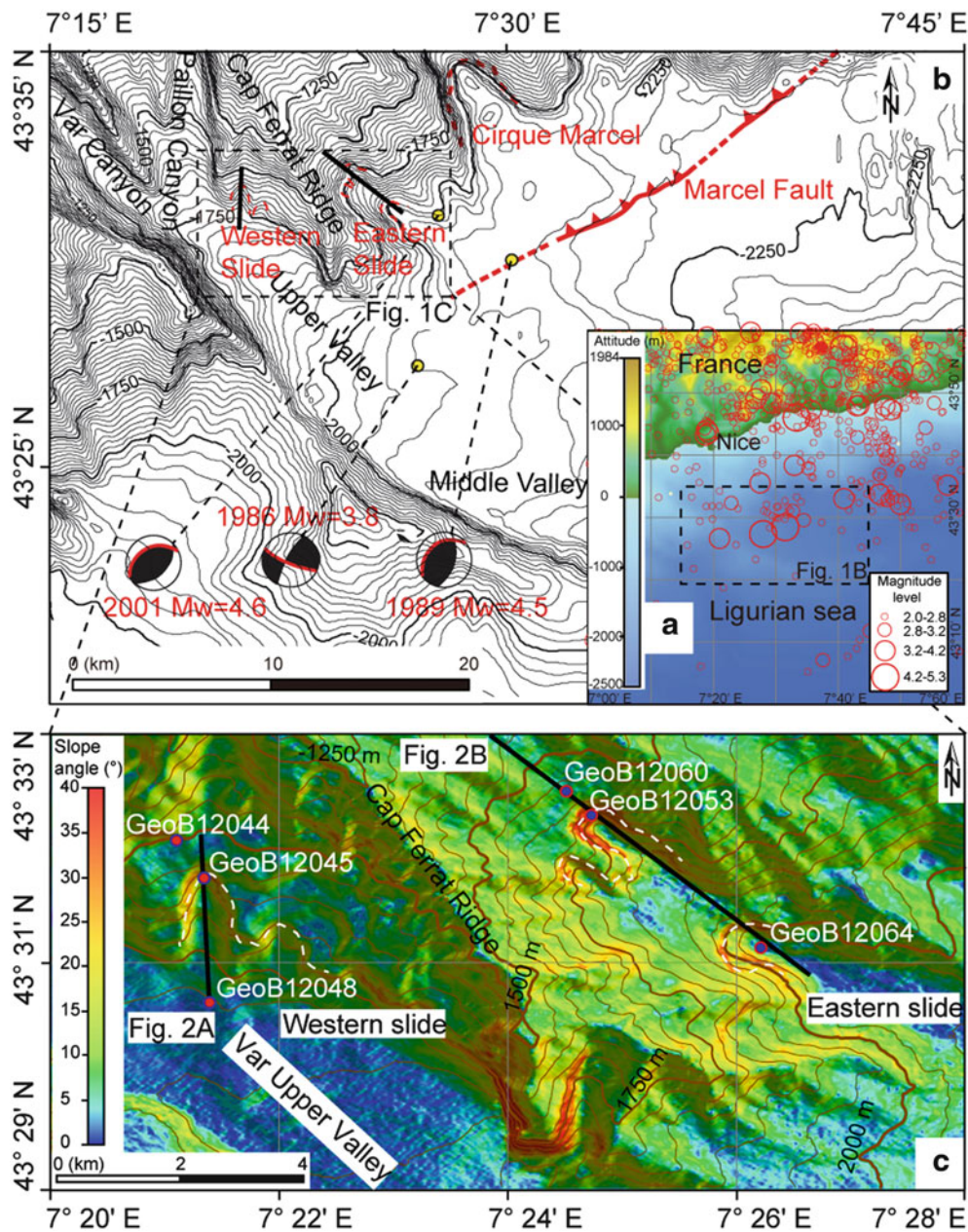
Fig. 1 (**a**) Map showing the location of the study area, *red circles* indicate earthquake records of the Ligurian margin from 1980 to 2010 (catalogue from the Bureau Central Sismologique Français). (**b**) Bathymetric map of deeper slope of Ligurian margin with focal mechanisms of the moderate earthquakes associated with the Marcel Fault (taken from Larroque et al. 2012). (**c**) Slope-gradient map of WS and ES. *Circles* indicate core locations. *Dashed white lines* mark the headwalls of both slides (revised after Förster et al. 2010). *Black lines* indicate the locations of seismic profiles shown in Fig. 2b

Grain size distribution analysis using the Beckman Coulter LS 13320 particle size analyzer and Atterberg limits using the Casagrande apparatus and rolling thread method were carried out. Oedometer tests were performed using a GIESA uniaxial incremental loading oedometer system. The drained sediment strength parameters (cohesion c′ and internal friction angle φ′) were determined using a displacement-controlled direct shear apparatus built by GIESA (Germany).

Slope Stability Analysis

The 1D infinite slope stability analysis is used to calculate the factor of safety (FS). For static conditions the FS calculation after Morgenstern (1967) follows:

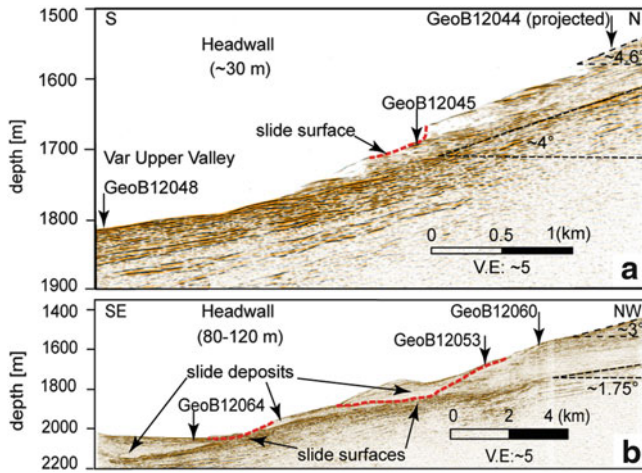$$FS = \frac{S_u}{\gamma' z \sin\theta \cos\theta} \quad \text{(undrained)} \qquad (1)$$

Fig. 2 Seismic profiles of WS (**a**) and ES (**b**) (modified after Förster et al. 2010). Note that the bulge in *panel* B does not show the real morphology of the headwall but is an artefact because the profile crosses the flank of slope
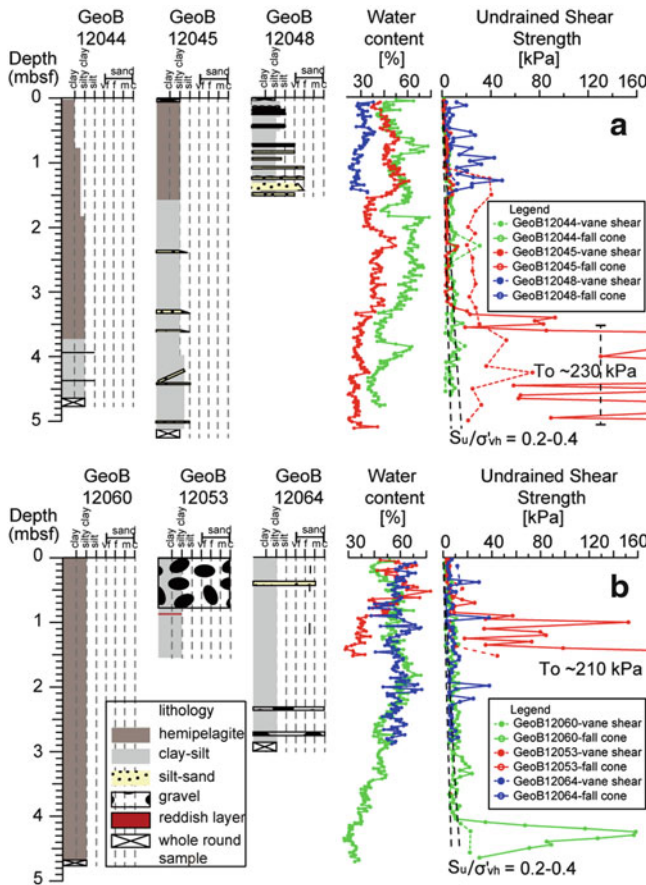

Fig. 3 Lithology, Water content as representative for physical properties and undrained shear strength of the sediments from WS (**a**) and ES (**b**)

$$FS = \frac{c' + \gamma'z(\cos^2\theta - \lambda*)\tan\phi'}{\gamma'z\sin\theta\cos\theta} \quad \text{(drained)} \quad (2)$$

Where θ is slope angle and $\lambda*$ is overpressure ratio ($\lambda* = \Delta u/\sigma'_{vh}$), Δu is overpressure, σ'_{vh} is vertical effective stress for hydrostatic conditions ($\sigma'_{vh} = \gamma'z$). γ' is buoyant weight, z is overburden depth.

Pseudostatic analysis was used for evaluation of slope stability under earthquake, which is assumed the integrated horizontal ground acceleration k g (where k is the seismic coefficient and g is the acceleration due to gravity) to be applied over a time period long enough for the induced shear stress to be considered constant while the overpressure that may be generated during an earthquake is not taken into account for the slope stability analysis (see Mulder et al. 1994):

$$FS = \frac{S_u}{\gamma'z[\sin\theta\cos\theta + k(\gamma/\gamma')\cos^2\theta]} \quad \text{(undrained)} \quad (3)$$

$$FS = \frac{c' + \gamma'z(\cos^2\theta - \lambda*)\tan\phi'}{\gamma'z[\sin\theta\cos\theta + k(\gamma/\gamma')\cos^2\theta]} \quad \text{(drained)} \quad (4)$$

Where γ is unit weight.

Results

Physical and Geotechnical Properties

Water content and undrained shear strength of sediments are presented in Fig. 3. Sediments from undeformed slopes have high values of water content (~60 %), while lower values (~30 %) are seen in deeper parts of sediment cores from the headwall. Sediments from the ES deposit area have similar water content as sediments from the undeformed upslope region. Low water content (~30 %) of sediments from the deposit area of WS is attributed to coarse-grained materials. Undrained shear strength of sediments from undeformed slope gradually increase with depth to ~20 kPa at 5 m core depth with value of S_u/σ'_{vh} ranging between 0.2 and 0.4 which indicate normal consolidated state for marine sediments (Cochonat et al. 1993) Sediments from headwall have low shear strength (0–20 kPa) and increase rapidly up to ~200 kPa at 3.65 m for WS and 1.o m for ES.

The dominant lithology is clayey silt (with ~20 % clay) with an intermediate plasticity according to our Atterberg limit measurements. Oedometer tests indicate sediment from the undeformed slope of WS is underconsolidated (overconsolidation ratio (OCR) = $\sigma'_{pc}/\sigma'_{vh}$) = 0.62, $\lambda* = 1—OCR$ = 0.38) and normally consolidated (OCR = 0.99, $\lambda* = 0$)
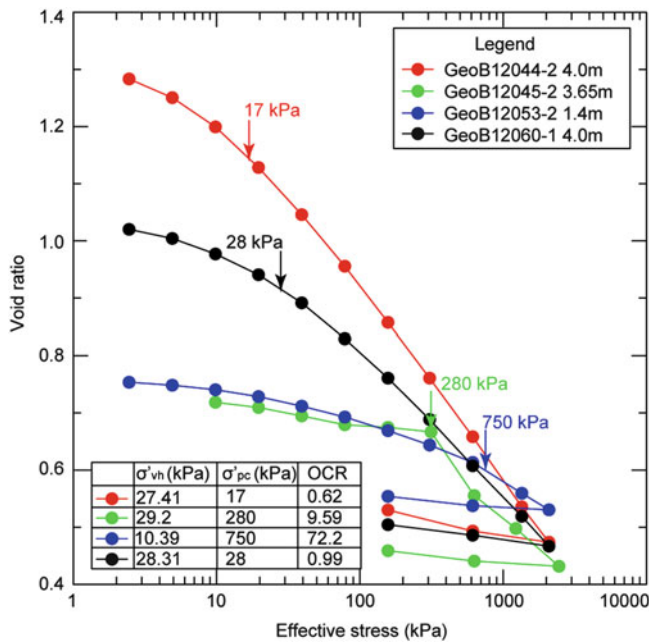
Fig. 4 e-log (σ'_v) curves from oedometer tests with calculated preconsolidation stress (σ'_{pc}) and overconsolidation ratio (OCR)

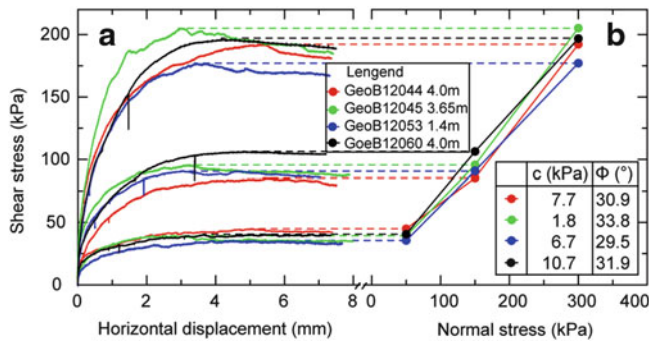**Fig. 5** (**a**) Direct shear test protocols shown as shear stress versus horizontal displacement. (**b**) Mohr-Coulomb failure planes obtained from peak shear strength values

for ES whereas sediments below the slip surface near the headwall are strongly overconsolidated (OCR = 9.6 for WS, OCR = 72.2 for ES) (Fig. 4). The calculated thickness of removed overburden material are 31 m for WS and 100 m for ES using the equation of Silva et al. (2001). This is consistent with the depth estimates based on seismic profiles (Fig. 2). Drained direct shear test results are presented in Fig. 5. Values of c' are lower in sediments from WS (1.8–7.7 kPa) than in ES (6.7–10.7 kPa) whereas values of ϕ' are slightly higher in sediments from WS (30.9–33.8°) than in ES (29.5–31.9°).

Slope Stability Analysis

Factors of safety for four different scenarios were calculated using Eqs. (1–4) with two parameters changing within a certain range while all others were kept constant (for details see Table 1). The undrained shear strength-depth relation was obtained using fall cone tests data with linear regression. We assume λ* of WS is 0.38 due to underconsolidated state and no overpressure in ES because of its normal consolidation state. Our data suggest that both slopes appear to be presently stable under both undrained and drained static conditions. The results further indicate that the slope angle has a stronger influence on slope stability than slope failure depth (Fig. 6). The minimum horizontal acceleration coefficient required to trigger slope failure (FS = 1) was back-calculated based on Eqs. (3) and (4). For the undrained earthquake case, a value of k = 0.08 is needed to trigger slope failure for ES, while a lower value of k = 0.06 is needed to fail the WS slope.

Discussion

Preconditioning Factors of WS and ES: Superficial Failure vs. Deep-Seated Failure

WS is affected by superficial failures with shallow headwall (~30 m vertical displacement) while ES shows deep-seated failure with deeper scars (~100 m). Previous studies in the Ligurian margin have shown that the slope angle is a governing factor for sediment failure (e.g. Cochonat et al. 1993 and Migeon et al. 2011). High slope angles (>5°) promote regular small-volume failure events, which prevent the area to build a thick, potentially unstable sediment package. Sedimentation rates are assumed to be higher near WS on the flank of Var Upper Valley than in the ES region due to regular sediment supply by hyperpycnal flows (Klaucke et al. 2000). On the other hand, hyperpycnal flows are also involved in the gradual undercutting at the base of canyon walls leading to local oversteepening (Migeon et al. 2011). High slope angles with high sedimentation rates and effect of hyperpycnal flows promote superficial failure in WS whereas relative lower slope angle, lower sedimentation rates and without reworking by bottom currents promote the accumulation of a thick but more stable sediment succession in the ES region. The latter then serve as prerequisite and sufficient material resources for deep-seated failure and larger volumes of slid material.

Table 1 Parameters used for slope stability calculations

Parameter	WS GeoB12044				ES GeoB12060			
	US	DS	UE	DE	US	DS	UE	DE
S_u (kPa)	1.46z +3.3	32.5			1.7z +5.0	260.0		
z (m)	*1–50*	30			*1–300*	100		
θ(°)	*1–10*				*1–10*			
c′(kPa)	–	5	–	5	–	9	–	9
φ′(°)	–	32	–	32	–	30	–	30
γ(kN/m²)	–		17.1		–		17.4	
λ*	–	0.38	–	0.38	–	0	–	0
k	–		*0–0.1*	*0–0.3*	–	–	*0–0.1*	*0–0.3*
γ′(kN/m²)	7.31				7.62			
g (m/s²)	9.81				9.81			
FS/	2.8/	>7/	1/	1/	4.5/	>7/	1/	1/
k	–	–	0.06	0.14	–	–	0.08	0.23

US Undrained Static, *DS* Drained Static, *UE* Undrained Earthquake, *DE* Drained Earthquake, numbers in italics indicate variable parameters
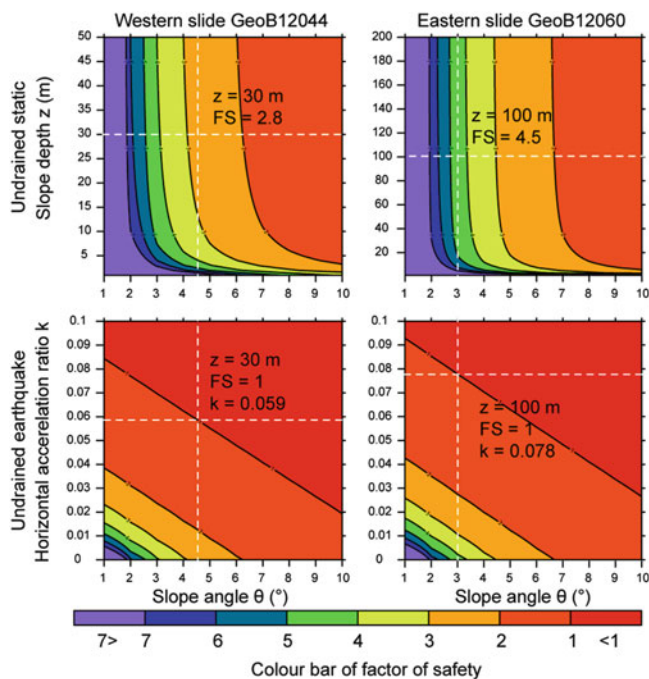

Fig. 6 Undrained slope stability analyses and back-calculations of pseudostatic horizontal acceleration ratio for WS (GeoB12044) and ES (GeoB12060). *Dashed white lines* indicate current mean values of the parameters for static analysis and values of pseudostatic horizontal acceleration required to trigger slope failure (FS = 1)

Fig. 7 PGA estimates using an empirical attenuation equation after Bindi et al. (2011). *Dashed white lines* indicate the 2001 earthquake and the distances between the slope scarps of WS and ES to the epicenter of the 2001 earthquake. *Red lines* indicate the PGA needed to currently trigger slope failure at WS and ES

The Influence of Earthquake to the Slope Stability

Superficial failures frequently occur in oversteepened, underconsolidated sediments resulting from high sedimentation rates, while deep-seated failures probably require external constraints such as seismic loading on the sediments to induce slope instability. When considering acceleration-induced earth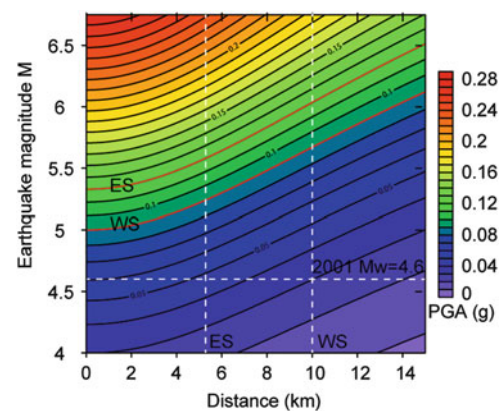quakes as a static parameter, it is reasonable to assume a drained pseudostatic model (Mulder et al. 1994). Critical pseudostatic acceleration as the average equivalent uniform shear stress imposed by seismic shaking represents ~65 % of the effective seismic peak ground acceleration (PGA) (Strasser et al. 2011). WS is more vulnerable in undrained conditions where a PGA of 0.09 g (PGA = 0.06 g/0.65) is sufficient to fail the slope. In our study, PGA has been estimated using an empirical attenuation equation after Bindi et al. (2011) (Fig. 7). Over the past 30 years, earthquakes with magnitudes 3.8–4.6 have occurred around the Marcel Fault in distances as close as 10 km to WS and 5.6 km to ES (Larroque et al. 2012 and Fig. 1b). Despite this short epicentral distance, PGA induced by the M4.6 2001 earthquake (0.03 g for WS and 0.05 g for ES) is still insufficiently strong to trigger instability in either WS or ES. The attenuation relationship indicates that moderate earthquake activity of M5.0 on the

spot or stronger earthquakes (e.g. M = 6.1) in epicentral distances <15 km are required to fail the WS slope. In the ES area, moderate earthquakes with M 5.3 on the spot or >M6.5 earthquakes at distances <15 km are required to trigger slope failure. From Mulder et al. 1994, PGA ranging from 0.095 g to 0.26 g could be expected for earthquakes with return periods ranging from 100 to 1,000 years, respectively. We propose that seismic triggers may have been required for the deep-seated failure in the ES area, but certainly also affected the instability of superficial failure in the WS region.

Conclusions

In summary, we have demonstrated how geotechnical properties of sediments and slope stability analysis of two distinct types of slope failure (superficial failure and deep-seated failure) control the Ligurian Margin. Consolidation test results can be used to calculate the amount of sediment removed by slope failure, which is consistent with depth estimates from seismic profiles. The slope angle seems to have a stronger influence on slope instability than slope failure depth below seafloor. For better assessment the potential instability in this tectonic active area, dating of different failure events is mandatory to correlate these data to real seismic events. However, the risk assessment shows that a large-size failure only requires moderate earthquake magnitudes, similar to (or even lower than) those of the 1887 historical event. Given the societal loss associated with a tsunamigenic landslide at the French Riviera, more detailed work has to be carried out in this direction.

References

Bindi D, Pacor F, Luzi L, Puglia R, Massa M, Ameri G, Paolucci R (2011) Ground motion prediction equations derived from the Italian strong motion database. Bull Earthquake Eng 9(6):1899–1920

Cochonat P, Bourillet JF, Savoye B, Dodd L (1993) Geotechnical characteristics and instability of submarine slope sediments, the nice slope (N-W Mediterranean Sea). Mar Georesour Geotechnol 11(2):131–151

Dan G, Sultan N, Savoye B (2007) The 1979 Nice harbour catastrophe revisited: trigger mechanism inferred from geotechnical measurements and numerical modelling. Mar Geol 245 (1–4):40–64

Förster A, Spieß V, Kopf AJ, Dennielou B (2010) Mass wasting dynamics at the deeper slope of the Ligurian margin (Southern France). Submarine mass movements and their consequences andvances in natural and technological hazard research. Springer, Dordrecht, Heidelberg, London, New York, pp 66–77

Klaucke I, Cochonat P (1999) Analysis of past seafloor failures on the continental slope off Nice (SE France). Geo-Mar Lett 19 (4):245–253

Klaucke I, Savoye B, Cochonat P (2000) Patterns and processes of sediment dispersal on the continental slope off Nice, SE France. Mar Geol 162(2–4):405–422

Kopf A, Cruise Participants (2008) Report and preliminary results of Meteor Cruise M 73/1: LIMA-LAMO (Ligurian Margin Landslide Measurements & Observatory). Berichte Fachbereich Geowissenschaften, Universität Bremen, 264; 161p

Larroque C, Scotti O, Ioualalen M (2012) Reappraisal of the 1887 Ligurian earthquake (western Mediterranean) from macroseismicity, active tectonics and tsunami modelling. Geophys J Int 190(1):87–104

Leynaud D, Sultan N (2010) 3-D slope stability analysis: a probability approach applied to the nice slope (SE France). Mar Geol 269 (3–4):89–106

Locat J, Lee HJ (2002) Submarine landslides: advances and challenges. Can Geotech J 39(1):193–212

Migeon S, Cattaneo A, Hassoun V, Larroque C, Corradi N, Fanucci F, Dano A, Mercier de Lepinay B, Sage F, Gorini C (2011) Morphology, distribution and origin of recent submarine landslides of the Ligurian Margin (North-western Mediterranean): some insights into geohazard assessment. Mar Geophys Res 32(1–2):225–243

Morgenstern N (1967) Submarine slumping and the initiation of turbidity currents. Mar Geotechnique 189–220

Mulder T, Tisot J-P, Cochonat P, Bourillet J-F (1994) Regional assessment of mass failure events in the Baie des Anges, Mediterranean Sea. Mar Geol 122(1–2):29–45

Silva AJ, LaRosa P, Brausse M, Baxter CD, Bryant WR (2001) Stress states of marine sediments in plateau and basin slope areas of the northwestern Gulf of Mexico. Offshore Technology Conference

Stegmann S, Sultan N, Kopf A, Apprioual R, Pelleau P (2011) Hydrogeology and its effect on slope stability along the coastal aquifer of Nice, France. Mar Geol 280(1–4):168–181

Strasser M, Hilbe M, Anselmetti F (2011) Mapping basin-wide subaquatic slope failure susceptibility as a tool to assess regional seismic and tsunami hazards. Mar Geophys Res 32 (1–2):331–347

Sultan N, Cochonat P, Canals M, Cattaneo A, Dennielou B, Haflidason H, Laberg JS, Long D, Mienert J, Trincardi F, Urgeles R, Vorren TO, Wilson C (2004) Triggering mechanisms of slope instability processes and sediment failures on continental margins: a geotechnical approach. Mar Geol 213(1–4):291–321